# Generic role of zeolite in enhancing anaerobic digestion and mitigating diverse inhibitions: Insights from degradation performance and microbial characteristics

Xiaoqing Wang, Vincent Dürr, Angéline Guenne, Laurent Mazéas, Olivier Chapleur

Journal of Environmental Management 356 (2024) 120676

Contents lists available at ScienceDirect

Journal of Environmental Management

journal homepage: www.elsevier.com/locate/jenvman

Research article

# Generic role of zeolite in enhancing anaerobic digestion and mitigating diverse inhibitions: Insights from degradation performance and microbial characteristics

Xiaoqing Wang, Vincent Dürr, Angéline Guenne, Laurent Mazéas, Olivier Chapleur *

*Université Paris-Saclay, INRAE, PRocédés biOtechnologiques au Service de l'Environnement, 92761, Antony, France*

ARTICLE INFO

Handling editor: Lixiao Zhang

*Keywords:*
Anaerobic digestion
Zeolite
Mitigation
16S rRNA gene sequencing
Common components analysis

ABSTRACT

Zeolite was shown to mitigate anaerobic digestion (AD) inhibition caused by several inhibitors such as long-chain fatty acids, ammonia, and phenolic compounds. In this paper, we verified the genericity of zeolite's mitigating effect against other types of inhibitors found in AD such as salts, antibiotics, and pesticides. The impacts of inhibitors and zeolite were assessed on AD performance and microbial dynamics. While sodium chloride and erythromycin reduced methane production rates by 34% and 32%, zeolite mitigated the inhibition and increased methane production rates by 72% and 75%, respectively, compared to conditions without zeolite in the presence of these two inhibitors. Noticeably, zeolite also enhanced methane production rate by 51% in the uninhibited control condition. Microbial community structure was analyzed at two representative dates corresponding to the hydrolysis/fermentation and methanogenesis stages through 16S rRNA gene sequencing. The microbial characteristics were further evidenced with common components analysis. Results revealed that sodium chloride and erythromycin inhibited AD by targeting distinct microbial populations, with more pronounced inhibitory effects during hydrolysis and VFAs degradation phases, respectively. Zeolite exhibited a generic effect on microbial populations in different degradation stages across all experimental conditions, ultimately contributing to the enhanced AD performance and mitigation of different inhibitions. Typically, hydrolytic and fermentative bacteria such as *Cellulosilyticum*, *Sedimentibacter*, and *Clostridium sensu stricto* 17, VFAs degraders such as *Mesotoga*, *Syntrophomonas*, and *Syntrophobacter*, and methanogens including *Methanobacterium*, *Methanoculleus*, and *Methanosarcina* were strongly favored by the presence of zeolite. These findings highlighted the promising use of zeolite in AD processes for inhibition mitigation in general.

## 1. Introduction

With rapid urbanization and economic development, organic waste management is now a major environmental and economic challenge for many municipal utilities (Lee et al., 2020; Xiao et al., 2022). Commonly referred to as "biowaste", these organic wastes come from various origins, including agricultural by-products (manure, straw, silage), household and food industry wastes, sludge from wastewater treatment plants, and green wastes from parks and gardens. Among the various biowaste management methods, anaerobic digestion (AD) is one of the most popular, as it simultaneously achieves biowaste stabilization and nutrient recovery and reduces the burden on fossil fuels by producing biogas (mainly methane) which can be used as clean energy (Lee et al., 2020).

The degradation of organic wastes in AD is accomplished by a series of interconnected microorganisms. The efficiency and stability of AD highly rely on the composition and activity of these intricate microbial communities, which can be easily impacted by perturbations (Li et al., 2018). In addition to the instability due to improper technical parameters, various compounds can be potential inhibitors warranting attention.

Considering that food waste, agricultural waste, and livestock waste are important substrates for AD, careful consideration should be given to potential inhibitors that may be present in these substrates. The high salinity in food waste, particularly sodium chloride derived from extensive use of food flavorings, poses a significant challenge for AD (Li et al., 2023). Although salts at reasonable concentrations benefit microbial growth, high salinity leads to high-osmolarity conditions,

* Corresponding author.
*E-mail address:* olivier.chapleur@inrae.fr (O. Chapleur).

https://doi.org/10.1016/j.jenvman.2024.120676
Received 16 January 2024; Received in revised form 4 March 2024; Accepted 13 March 2024
Available online 22 March 2024

causing decreased enzyme catalytic rate, dehydration, or even death of microbial cells (Onodera et al., 2017; Li et al., 2023). Pesticides used on crops or antibiotics used to treat livestock can end up in an anaerobic digester when agricultural waste or manure is introduced as substrate. These organic compounds are usually poorly soluble in water and readily bind to bacterial cell membranes, causing the cells to no longer be able to metabolize (Schnürer and Jarvis, 2018). The toxicity and inhibition of several pesticides (malathion, fenitrothion, methoxychlor, and chlorfenvinphos) and antibiotic residues (tetracycline, erythromycin, sulphonamides, and norfloxacin) on anaerobic microbial consortia have been reported in Sadecka et al. (2016), Liu et al. (2021), Gaballah et al. (2023), and Zhang et al. (2023). Exposure to antibiotics can also lead to the dominance of antibiotic-resistant bacteria within the microbial community and a decrease in microbial diversity, reducing the stability of AD process (Oliver et al., 2020). Even though methanogens are generally less sensitive to antibiotics than bacteria, the biogas process can also be interrupted by the fact that fermentative or acetic acid-forming bacteria are inhibited, leading to the accumulation of fatty acids and a decrease in pH (Aydin et al., 2015; Schnürer and Jarvis, 2018).

Several strategies have been developed to avoid or alleviate AD inhibition, such as substrate pretreatment, acclimation of the inoculated microorganisms, co-digestion of different sources of organic wastes, and addition of support materials (Cardona et al., 2019; Abdallah et al., 2022; Balasundaram et al., 2022). Among these, support materials addition is gaining popularity because it is easier to implement with satisfying effects. Many types of support materials have been tested in AD such as activated carbon, biochar, magnetite, and minerals (Montalvo et al., 2012; Yin et al., 2020). In particular, zeolite, an aluminosilicate mineral, is a promising material. Its microporous structure provides a surface to develop biofilms and enrich microbial communities, while also functioning as a repository to preserve essential nutrients like potassium, sulfur, and other trace elements crucial for microbial metabolism (Nakhli et al., 2017; Tang et al., 2023). Zeolite has shown potential for alleviating ammonia inhibition in AD. This is attributed to its cation exchange capacity, which reduces ammonia concentration via a $Ca^{2+}/NH_4^+$ exchange mechanism (Montalvo et al., 2012), as well as its ability to enhance syntrophic propionate oxidation (Cardona et al., 2021). In addition to ammonia, zeolite mitigated the inhibition caused by phenol and excessive production of long-chain fatty acids, attributed to its role in preserving methanogenic communities (Poirier et al., 2018; Nordell et al., 2013).

Considering the friendly cost of natural zeolite and its ability to mitigate several inhibitions, it motivates further exploration into the general applicability of zeolite to other types of inhibitory compounds, including the ionic compound sodium chloride and other categories of organic compounds such as pesticides and antibiotics.

For this purpose, we chose three different molecules of inhibitors: sodium chloride, S-metolachlor (the S-enantiomer of metolachlor, a widely used herbicide), and erythromycin (widely used in livestock farming to prevent and treat various diseases) to assess zeolite's potential in mitigating these inhibitions. Throughout the experiment, the degree of inhibition and the effectiveness of zeolite in mitigating the inhibitory impacts were evaluated by regularly monitoring degradation performance (gas production and chemical indicators in the digesters) and analyzing microbial characteristics at specific time points representing different stages of the process.

## 2. Material and methods

### 2.1. Experimental setup

Twenty-four lab-scale digesters of 1000 mL with a working volume of 700 mL were set up, inoculated with 5.7 g of centrifuged methanogenic sludge and fed with 12.7 g of mashed biowaste to reach a substrate/inoculum ratio of 0.79 g COD/0.18 g COD. The inoculum was sampled from a 60 L laboratory anaerobic bioreactor fed with the same biowaste. The biowaste was collected from the restaurant of our research institute. A biochemical potential buffer (ISO 11734 (1995)) solution was added to reach the final working volume. The composition of the buffer solution is detailed in Supplementary Material. All digesters were finally supplemented with 11.76 g/L of $NaHCO_3$ to buffer the pH.

Eight conditions were tested in triplicate. In the first series of 12 digesters, different compounds were added to create the inhibition: 20 g/L of sodium chloride (NaCl, Acros Organics), 400 mg/L of erythromycin (ERY, Acros Organics), 5 mg/L of S-metolachlor (MET, Honeywell), and a control group without inhibition. The concentrations of inhibitors were determined based on literature and our preliminary test with the same substrate and inoculum (Chen et al., 2014; Ozbayram et al., 2015; Zhang et al., 2023). A second series was set up exactly as the first one but with 15 g/L of zeolite (Siliz 24, Somez, France) added. All digesters were sealed with a rubber septum and incubated at 35 °C without agitation.

Liquid samples (8 mL) were taken weekly and centrifuged at 10,000 g for 10 min. Supernatants and pellets were separated and stored at −20 °C. Gas samples (7 mL) were taken regularly for isotopic analyses.

### 2.2. Biogas production analyses

The biogas accumulated in the headspace was drained regularly, and the pressure in the digesters was measured with a differential manometer (Digitron, 2082P) to calculate the volume of gas produced. The biogas composition was simultaneously analyzed using micro-GC (CP4900, Varian) to quantify the percentages of methane and carbon dioxide, according to Chapleur et al. (2016). The gas production of each digester was modeled using the Gompertz equation (Eq. 1) with Grofit R package:

$$y(t) = A * \exp\left[-\exp\left(\mu \frac{e}{A(\lambda - t)} + 1\right)\right] \quad (1)$$

where y(t) represents the cumulative production (mgC) at day t, A is the ultimate production (mgC), μ is the maximum production rate (mgC/day), and λ is the lag phase (days).

The accuracy of the modeling was evaluated by calculating the average relative difference (ARD) using Eq. (2):

$$ARD(\%) = \frac{1}{n}\sum_{i=1}^{n}\frac{\left|\chi_{pi} - \chi_{ei}\right|}{\chi_{ei}} * 100 \quad (2)$$

where n is the number of sampling times, $\chi_p$ is the predicted value by the model, and $\chi_e$ is the corresponding experimental value. For consistency, measurements before lag phase were excluded from the ARD calculation.

The apparent isotopic factor ($\alpha_{app}$) was used as an indicator of the dominant methanogenic pathway and calculated using Eq. (3):

$$\alpha_{app} = \frac{\delta^{13}CO_2 + 10^3}{\delta^{13}CH_4 + 10^3} \quad (3)$$

$\delta^{13}CH_4$ and $\delta^{13}CO_2$ represent the isotopic composition of methane and carbon dioxide, measured using a Trace Gas Chromatograph Ultra (Thermo Scientific) coupled to an isotope ratio mass spectrometer Delta V Plus (Thermo Scientific) through a combustion machine GC III (Thermo Scientific) (Cardona et al., 2019). In general, a value of $\alpha_{app} > 1.065$ suggests that the hydrogenotrophic pathway is dominant, while a value of $\alpha_{app} < 1.055$ indicates that acetoclastic is the primary methanogenesis pathway (Conrad, 2005).

### 2.3. Chemical analyses

pH of the liquid samples was measured with a pH meter (HANNA).

Volatile Fatty Acids (VFAs) concentrations were measured by ionic chromatography (ICS 5000+, Thermo Fisher Scientific) equipped with IonPAc ICE-AS1 column (9 mm 250 mm) (Cardona et al., 2019). Dissolved organic and inorganic carbon (DOC and DIC) were measured using a TOC-L CPN analyzer (Shimadzu) following the French standard NF EN 1484.

From day 0 to day 34, the MET concentration in the supernatant samples from MET condition was quantified by liquid chromatography coupled to mass spectrometry (LC-MS) using an Accela 1250 pump system connected to an LTQ Orbitrap XL mass spectrometer (Thermo Fisher Scientific). Before the quantification, a standard MET solution with a concentration gradient from 0.5 to 100 μg/L was prepared in the BMP buffer to measure its signal response and create a standard curve. The MET concentration in the samples was determined using the standard curve. Methods for quantifying erythromycin in the laboratory have yet to be developed. In the case of NaCl, its concentration was assumed to remain constant throughout the experiment.

### 2.4. Microbial community monitoring

16S sequencing was performed on two selected dates. The first date corresponding to the peak of VFAs accumulation targeted the hydrolysis and acidogenesis processes, referred to as early degradation stage. The second date corresponding to the peak of biogas production focused on the methanogenesis process, referred to as late degradation stage. The date selection was based on the actual performance of each digester, meaning that the chosen dates could vary depending on different conditions or replicates. In addition, 4 samples taken on day 0 from random digesters were also sequenced as representative of the inoculum. 52 samples were analyzed in total.

Total genomic DNA was extracted from the pellet samples using DNeasy PowerSoilPro Isolation Kit (Qiagen) with the QIAcube Instrument according to the manufacturer's instructions. The concentration of extracted DNA was quantified with Qubit 2.0 fluorometer using dsDNA kit (Invitrogen) and the purity was checked with Epoch 2 Microplate Spectrophotometer (Agilent BioTek).

The DNA was used for the amplification of the bacterial and archaeal hypervariable region V4–V5 of the 16S rRNA genes with fusion primers 515F (5′-GTGYCAGCMGCCGCGGTA-3′) and 928R (5′-CCCCGYCAATTCMTTTRAGT-3′). The library preparation is described in Madigou et al. (2019). Sequencing was performed on Ion Torrent Personal Genome Machine using Ion 316 chip and the Ion PGM Sequencing 400 Kit according to the manufacturer's instructions. The sequencing data for this study have been deposited in the European Nucleotide Archive (ENA) at EMBL-EBI under accession number PRJEB65129 (https://www.ebi.ac.uk/ena/browser/view/PRJEB65129).

### 2.5. Statistical analysis of microbial data

The sequencing data were processed using Torrent Suite software to export high-quality data in FastQ format. The FastQ data were analyzed using the FROGS bioinformatics pipeline (Escudié et al., 2018). Taxonomic affiliation was finally generated using BLAST and silva_138.1_16S_pintail100 database.

To ensure robustness and focus on the most relevant OTUs, OTUs with a total sequence count beyond 50 across all samples and present in at least half of the samples were retained. Following this filtration, the initial 941 OTUs were reduced to 436. The sequencing data were scaled with total sum scaling (TSS) to obtain each OTU's relative abundance within the sample, followed by mean centering and normalization for Common Components Analysis (CCA).

CCA is an unsupervised analysis method that extends the principles of PCA and enables simultaneous analysis of multiple data blocks (Bouhlel et al., 2018). In our analysis, individual OTUs were treated as distinct blocks. The dispersion pattern of the samples on the common components (CCs) was determined by the similarity in the OTUs' responses to the experimental factors, including zeolite, different inhibitors, and degradation stages. Subdominant OTUs were also considered as long as they influenced the sample dispersion. To highlight the most influential OTUs, on each CC, OTUs with loadings exceeding 2 standard deviations (±2 SD) were selected (Puig-Castellví et al., 2020). The selected OTUs were visually represented through a topological tree constructed using the phylogenetic information of these OTUs and generated using the GraPhlAn online tool accessible via the Galaxy website (http://huttenhower.sph.harvard.edu/galaxy/).

## 3. Results and discussion

### 3.1. Anaerobic digestion performances

During the degradation process, chemical parameters were monitored and are displayed in Fig. 1. Zeolite addition significantly impacted all experimental conditions, including the uninhibited control group. It considerably increased the gas production rate, leading to the advanced completion of the degradation process without altering the ultimate volume of biogas produced, which consisted of roughly $^{2}/_{3}$ methane and $^{1}/_{3}$ carbon dioxide. The accumulation of three VFAs, namely acetic acid, propionic acid, and butyric acid, was observed, which is typical for batch digesters that degrade biowaste (Cardona et al., 2021).

#### 3.1.1. Biogas production kinetics

The Gompertz equation, a widely-used mathematical model, was employed on the methane and carbon dioxide production data to differentiate between the various experimental conditions (Ware and Power, 2017). The modeling parameters and the accuracy assessed by ARD are presented in Table 1. The low ARD values indicate a good summary of the data.

Even if the final total biogas production reached approximately the same volume in each digester, the effect of zeolite and inhibitors was mainly observable in gas production rate (μ) and lag phase (λ). For methane production, in digesters without zeolite, the production rate of NaCl and ERY condition was reduced by 34% and 32% compared to the uninhibited control condition, with a prolonged lag phase of 10 and 5 days. MET did not exhibit an observable inhibitory effect. Zeolite noticeably mitigated the inhibition by NaCl and ERY, which increased the methane production rate by 72% and 75% and shortened the lag phase by 17 and 12.5 days, respectively. Moreover, zeolite promoted gas production under uninhibited conditions. In control condition, methane production rate increased by 51% and the lag phase was shortened by 8 days, while in MET condition, methane production rate increased by 34%. Surprisingly, the production rate in any condition with zeolite was always higher than that in the uninhibited control condition, indicating that 15 g/L of zeolite is beneficial for AD process in general.

Regarding carbon dioxide, a similar ultimate volume was achieved in all conditions. NaCl condition without zeolite exhibited the strongest inhibition with the lowest production rate, while the lag phase was unaffected. Zeolite addition tripled the production rate in NaCl condition and doubled it for the others, including control digesters, showing the great potential of zeolite to promote biogas production.

Interestingly, zeolite improved repeatability between the replicates, as shown by lower standard deviations represented with error bars in the presence of zeolite. Similar effects have been documented with iron-based nanoparticles addition in batch AD (Casals et al., 2021). It is possible that zeolite facilitated microbial growth due to its porous structure, thereby stabilizing their activity and resulting in more consistent biological processes.

#### 3.1.2. pH and VFAs production

pH is a crucial parameter to provide a comprehensive understanding of the different stages of AD. Across all conditions, the degradation of organic matter in biowaste into VFAs resulted in a drop in pH. The pH increased once VFAs were degraded to form methane and carbon

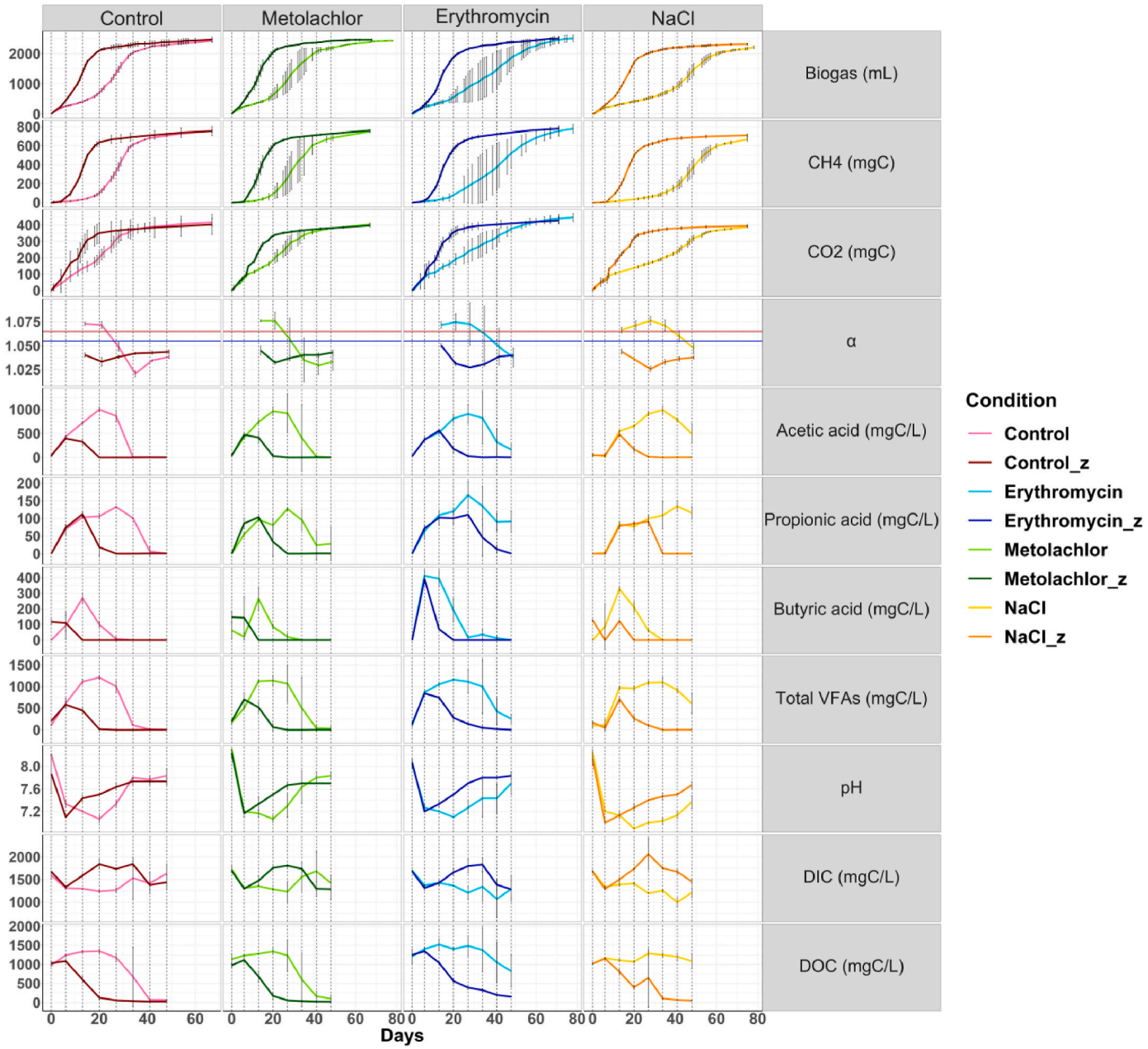


**Fig. 1.** Evolution of the chemical parameters in different conditions of inhibitors: total biogas production (mL), methane and carbon dioxide production (mgC), apparent isotope composition ($\alpha_{app}$), dissolved organic and inorganic carbon concentration (mgC/L), pH, acetic acid, propionic acid, butyric acid and total VFAs concentration (mgC/L). For $\alpha_{app}$, the blue and red horizontal lines show the limits for acetoclastic methanogenesis ($\alpha_{app} = 1.055$) and hydrogenotrophic methanogenesis ($\alpha_{app} = 1.065$). Vertical dashed lines show the dates of sampling. The data are the mean values for the triplicate digesters. Standard deviations are indicated with error bars. (For interpretation of the references to color in this figure legend, the reader is referred to the Web version of this article.)

dioxide. A significant difference was observed due to zeolite addition. Specifically, the zeolite resulted in a shorter decreasing period from three weeks to only one week. Additionally, the pH in conditions without zeolite remained lower than those with zeolite during the increasing period, suggesting VFAs accumulation, which may lead to inhibition.

The accumulation patterns of VFAs displayed variations among the conditions (Fig. 1). Acetic acid, the most abundant VFA and the easiest to metabolize by archaea, showed a peak concentration between day 7 and day 14, at around 500 mg C/L in all zeolite conditions. The peak concentration in conditions without zeolite was twice higher, suggesting more acetic acid accumulation. Furthermore, the acetic acid levels in ERY and NaCl conditions with zeolite reached 0 after 4 weeks, while without zeolite, acetic acid was still in the accumulation period at around 875 mg/L. The inhibitory effect on acetic acid degradation was particularly severe in NaCl condition, where the concentration was still 500 mg C/L after 7 weeks.

Butyric acid was the second most abundant VFA. Without zeolite, the levels of butyric acid increased up to 300 mg C/L, except for ERY, where it reached the highest accumulation of 400 mg C/L. With zeolite addition, the peak concentration only reached 100 mg C/L. In the case of ERY, zeolite did not reduce the peak concentration but accelerated its degradation. Butyric acid concentrations reached 0 earlier with zeolite regardless of the presence and type of inhibitor.

Propionic acid, the third most abundant VFA, is considered a “trouble-maker” due to its toxicity, which prevents microbes from converting it to methane (Li et al., 2020). Propionic acid was degraded in all cases after all other VFAs were degraded. However, there was a

**Table 1**
Gompertz parameters obtained after sigmoidal modeling of methane and carbon dioxide production and accuracy of modeling (ARD). Mean values and standard deviations were calculated for the triplicate digesters. "z" means condition with zeolite.

| | Conditions | Gompertz parameters | | | |
|---|---|---|---|---|---|
| | | μ (mgC/day) | λ (day) | A (mgC) | ARD (%) |
| **Methane production** | Control | 59.2 ± 0.7 | 13.9 ± 0.6 | 757.5 ± 15.2 | 6.5 ± 0.4 |
| | NaCl | 38.9 ± 1.6 | 24.3 ± 1.6 | 731.4 ± 15.1 | 7.4 ± 2.3 |
| | ERY | 40.2 ± 3 | 18.8 ± 6.4 | 811.4 ± 39.7 | 6.1 ± 2 |
| | MET | 58.6 ± 2.2 | 15.9 ± 3.8 | 754.3 ± 24.6 | 9.6 ± 3.8 |
| | Control_z | 89.3 ± 6.7 | 5.8 ± 0.4 | 717.8 ± 51 | 9.5 ± 6.7 |
| | NaCl_z | 66.9 ± 0.5 | 7.5 ± 0.2 | 688.1 ± 16.4 | 7.3 ± 0.3 |
| | ERY_z | 70.3 ± 3.6 | 6.3 ± 0.3 | 743.3 ± 5.4 | 5.9 ± 0.9 |
| | MET_z | 78.8 ± 3.4 | 6 ± 0.6 | 726.5 ± 11.6 | 8.5 ± 6.1 |
| **Carbon dioxide production** | Control | 19.3 ± 1 | 3.4 ± 2.3 | 436.2 ± 34 | 6.1 ± 0.6 |
| | NaCl | 9.5 ± 0.4 | 1.9 ± 0 | 544.5 ± 41.1 | 8.1 ± 0.4 |
| | ERY | 14 ± 5.6 | 3.4 ± 1.4 | 536.5 ± 115.1 | 5.2 ± 2.3 |
| | MET | 16.5 ± 2.9 | 2.7 ± 0.6 | 439.3 ± 49 | 5.9 ± 0.8 |
| | Control_z | 38.1 ± 0.7 | 2.7 ± 2.1 | 386.1 ± 61.5 | 3.6 ± 2.3 |
| | NaCl_z | 28.5 ± 1.1 | 2.6 ± 0.6 | 389.8 ± 7.8 | 5.2 ± 1.6 |
| | ERY_z | 33.7 ± 3.3 | 2.4 ± 1.6 | 413.6 ± 23.7 | 2.4 ± 0.4 |
| | MET_z | 32.5 ± 2 | 2.4 ± 0.4 | 383.1 ± 9.1 | 2.8 ± 0.5 |

longer period of accumulation without zeolite. Zeolite also lowered the maximum accumulation and accelerated the degradation in all conditions, which could be attributed to the enhanced propionate syntrophic oxidation observed by Cardona et al. (2021).

### 3.1.3. Dissolved organic and inorganic carbon

Fig. 1 shows the concentration of dissolved organic carbon (DOC) over time, which reflects the degradation of organic matter. At the start of the experiment, the DOC concentration was around 1000 mg C/L in all conditions. In conditions with zeolite, the DOC concentration showed a similar trend, with a slight increase due to VFAs production, followed by a sharp decrease over approximately four weeks. In conditions without zeolite, the DOC concentration remained stable during the first 3 weeks at a concentration between 1000 and 1500 mg C/L. From the fourth week, a decrease was observed in the control and MET conditions, while in the other two conditions, DOC concentrations decreased slowly from the fifth week and were still high (around 1000 mg C/L) at the end of the measurement due to inhibition on DOC consumers.

The dissolved inorganic carbon (DIC) levels in all conditions were very high, owing to the addition of $NaHCO_3$ as a pH buffer. In general, over the first 6 days of the experiment, the DIC levels decreased since the VFAs production caused a decline in pH. From the second week, the DIC levels increased in zeolite conditions while remaining relatively stable in non-zeolite conditions until the VFAs had been consumed. At the end of the measurement, DIC levels with and without zeolite tended to be close.

### 3.1.4. Isotopic analysis of biogas

The dominant methanogenic pathway was identified using $\alpha_{app}$, as shown in Fig. 1. Generally, an $\alpha_{app}$ greater than 1.065 suggests the hydrogenotrophic pathway is dominant, while a value less than 1.055 indicates the acetoclastic pathway is dominant (Conrad, 2005). In conditions without zeolite, $\alpha_{app}$ decreased rapidly during intensive methane production, indicating a switch to acetoclastic methanogenesis when acetate was available. However, the decrease of $\alpha_{app}$ was less conspicuous in ERY and NaCl conditions, possibly due to partial inhibition of acetoclastic methanogens. After the completion of acetic acid degradation, $\alpha_{app}$ increased again in control and MET conditions, occurring earlier than in the inhibited conditions, which could be attributed to the syntrophic propionate oxidation with hydrogenotrophic methanogens (Cardona et al., 2021). Considering the accelerated gas production rate, zeolite could have advanced the starting of acetoclastic methanogenesis.

### 3.1.5. S-metolachlor degradation

The evolution of MET concentration in the supernatant samples was presented in the Supplementary Material. Due to MET's hydrophobicity and lipotropy, it has the propensity to attach to the pellet, which may lead to unreliable quantification results. Indeed, the figure shows considerable disparities in initial concentrations among replicates, far from the expected concentration of 5000 μg/L initially introduced into the digesters. Besides, the zeolite condition has a lower initial concentration. As demonstrated by Ćwieląg-Piasecka et al. (2021), MET can bind with clay materials and their derivatives, such as zeolite in our study. A general disappearance of MET was observed everywhere, particularly within the first 3 weeks, which explained the observation of a very limited inhibition by MET. By day 20, the mean concentration of the triplicates decreased to 56 μg/L and 19 μg/L for conditions without and with zeolite, respectively. This decline corresponds to the increasing concentration of metolachlor ethanesulfonic acid and metolachlor oxalinic acid, recognized as MET metabolites (Munoz et al., 2011), thus providing evidence of MET rapid degradation.

## 3.2. Dominance of identified microbial populations

The relative abundance of bacterial and archaeal populations found in different digesters at family level is presented in Fig. 2. Since the sequencing results showed good repeatability between the replicates, the relative abundances used for the bar plots were mean values of the triplicates. All bacterial OTUs with a relative abundance of less than 1% in all samples are grouped into minor OTUs for better representation. The Supplementary Material presents bar plots plotted with data from each replicate. The relative abundance percentage of each OTU in each sample and the taxonomic affiliation are also provided. The microbial composition of the 4 samples randomly collected on day 0 was basically the same, indicating that the initial states of different digesters were similar, as expected.

In uninhibited control and MET conditions, the abundance of fermentative families *Clostridiaceae* and *Dysgonomonadaceae* increased compared to the inoculum in the early degradation stage, which is typical in AD processes. These families contain hydrolytic species and strongly correlate with VFAs production in AD treating food waste (Owusu-Agyeman et al., 2022). Zeolite maintained the amount of *Lachnospiraceae* and stimulated the growth of *Tannerellaceae* and *Sedimentibacteraceae*, known for their role in hydrolyzing and fermenting complex organic compounds (Yang et al., 2023). As the degradation progressed, the $H_2$-producing bacteria *Lentimicrobiaceae* emerged, which could account for the slight rise in $\alpha_{app}$ in control and MET conditions. *Syntrophomonadaceae* was stimulated by zeolite, which typically breaks down butyric acid to make it available for methanogens (Jannat et al., 2021).

In ERY condition, during the early degradation stage, the abundance of *Clostridiaceae* and *Dysgonomonadaceae* also increased. The *Peptostreptococcaceae* family exhibited a higher presence compared to other conditions, which could be attributed to the fact that members of this family, such as *Peptostreptococcus*, consist of Gram-positive bacteria known for their resistance to macrolides such as erythromycin

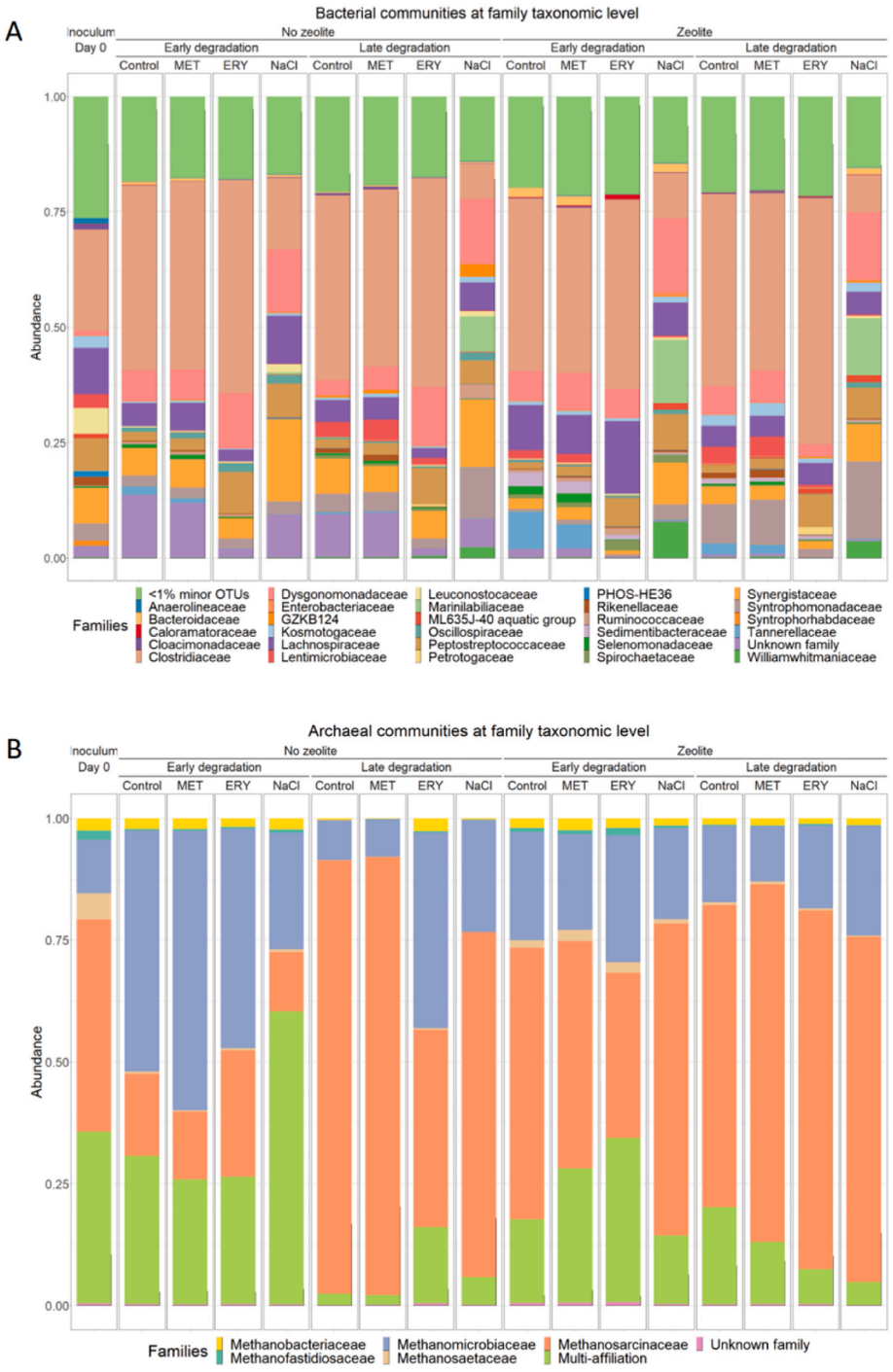


**Fig. 2.** Relative abundances of (A) bacterial and (B) archaeal families generated by 16S rRNA gene sequencing. Bacterial or archaeal OTUs of the same family are exhibited using the same color. The relative abundance displayed in each condition is the mean value of the triplicates. Bacterial OTUs with a relative abundance of less than 1% in all the samples are grouped into minor OTUs. The early and late degradation stages are represented by the two sampling dates at peaks of VFAs accumulation and biogas production, respectively, corresponding to the hydrolysis and methanogenesis stages. (For interpretation of the references to color in this figure legend, the reader is referred to the Web version of this article.)

(Goldstein, 2000; Ogbolu et al., 2018). Noticeably, *Lachnospiraceae* was inhibited by ERY but zeolite completely preserved this family, with a relative abundance of 18.64% even higher than the control (11.69%), suggesting a promoted hydrolysis stage by zeolite (Poirier et al., 2018). However, during the late stage, there was an inhibition on *Syntrophomonadaceae* and zeolite did not reduce this inhibition as effectively as in the other conditions. This could explain the higher accumulation level of butyric acid observed in the degradation performance under ERY condition, even when zeolite was added.

The microbial communities exhibited the most significant changes under the NaCl condition. The relative abundance of *Clostridiaceae* notably decreased to 19.74%, compared to 48.65% in the control condition, indicating a strong inhibition of this family and the hydrolysis process. However, *Synergistaceae* prominently resisted the NaCl inhibition and thrived. This family can convert acetate into $H_2$ and $CO_2$ and has already been detected in saline AD processes (Buenaño-Vargas et al., 2024). Interestingly, family *Marinilabiliaceae* occurred and thrived, especially faster with zeolite. *Syntrophomonadaceae* enriched in the late

degradation stage, with zeolite contributing to a 5.95% increase in its relative abundance. Similar findings were reported by Duan et al. (2020), highlighting the dominance of *Marinilabiliaceae* sp.3 and *Syntrophomonadaceae* sp.6 facing $K^+$ and $Na^+$ inhibition attributed to their stronger $Na^+$-tolerant ability. Cardona et al. (2021) also reported the preservation of *Marinilabiliaceae* by zeolite. Besides, zeolite promoted the growth of the fermentative *Williamwhitmaniaceae* family (Zheng et al., 2021).

Concerning archaeal communities, in conditions without zeolite, *Methanomicrobiaceae*, a group of hydrogenotrophic methanogens, initially dominated the early stage. But as VFAs accumulated, it was gradually replaced by *Methanosarcinaceae*. This shift occurred because *Methanomicrobiaceae* was sensitive to the accumulated VFAs, whereas *Methanosarcinaceae* primarily utilized acetate to produce methane, correlating with the decreased $\alpha_{app}$ (Lv et al., 2019). Zeolite generically promoted *Methanosarcinaceae* in the early stage across all conditions and mitigated the ERY and NaCl inhibition on it in the late stage, correlating with the accelerated acetic acid consumption and accounting for the dominated acetoclastic methanogenesis in zeolite conditions. The same findings were reported by Poirier et al. (2018), where zeolite preserved the major representative genus from *Methanosarcinaceae* family. Additionally, in the early stage, zeolite slightly stimulated the *Methanosaetaceae* family, which are also acetoclastic methanogens. This aligned with the $\alpha_{app}$ results showing that acetoclastic methanogenesis was clearly characteristic in the presence of zeolite. Perez-Perez et al. (2021) have observed a higher *Methanosaetaceae* presence when employing zeolite in an anaerobic expanded granular bed reactor treating synthetic swine wastewater, which could be related to zeolite's ability to improve interactions between the archaea and bacteria consortium.

### 3.3. Revealing the effects of the experimental factors on the microorganisms

#### 3.3.1. Comprehensive insights from common components analysis

The CCA scores of 48 samples (24 digesters and 2 degradation stages) on the first 4 components are illustrated in Fig. 3. The conventional CCA sample biplots are available in Supplementary Material.

On CC1, samples from control and MET conditions showed positive scores, while ERY and NaCl conditions exhibited negative scores, independently of zeolite addition or degradation stages. CC1 effectively separated the uninhibited and inhibited conditions, whatever the inhibitor was. It suggested a common effect of both inhibitors on the microbial community. More precisely, CC1 was descriptive of the performance levels of different conditions, with the uninhibited control condition with zeolite (performing the best) scoring the highest, and NaCl condition without zeolite (being the most inhibited) scoring the lowest, in line with the Gompertz modeling results.

CC2 further differentiated ERY condition displaying positive scores at the top and NaCl condition featuring negative scores at the bottom, indicating the differences in inhibitory effects of these two inhibitors on microbial populations. Besides, the effect of zeolite was more noticeable for ERY condition at the late stage.

A generic effect of zeolite on microbial populations was observed on CC3 and CC4, linked to degradation stages. On CC3, positive scores in the early stage were exclusively observed for all conditions with zeolite, indicating a shared effect of zeolite on microbial populations during the early stage. Similarly, CC4 featured positive scores for conditions with zeolite in the late stage. Furthermore, different zeolite conditions showed varying positive scores, implying that zeolite generically impacted the microbial populations across all conditions, but changes in microbial populations were also influenced by the presence and type of inhibitors.

#### 3.3.2. Key microbial populations specific to different experimental factors

On each CC, the OTUs with high loading values (>±2 SD) were chosen and depicted in the phylogenetic tree (Fig. 4). In total, 4 archaeal and 101 bacterial OTUs were selected, which can be considered the most characteristic OTUs for each CC and the specific experimental factors. Loading values of the selected OTUs on each CC and their S-plots can be found in the Supplementary Material.

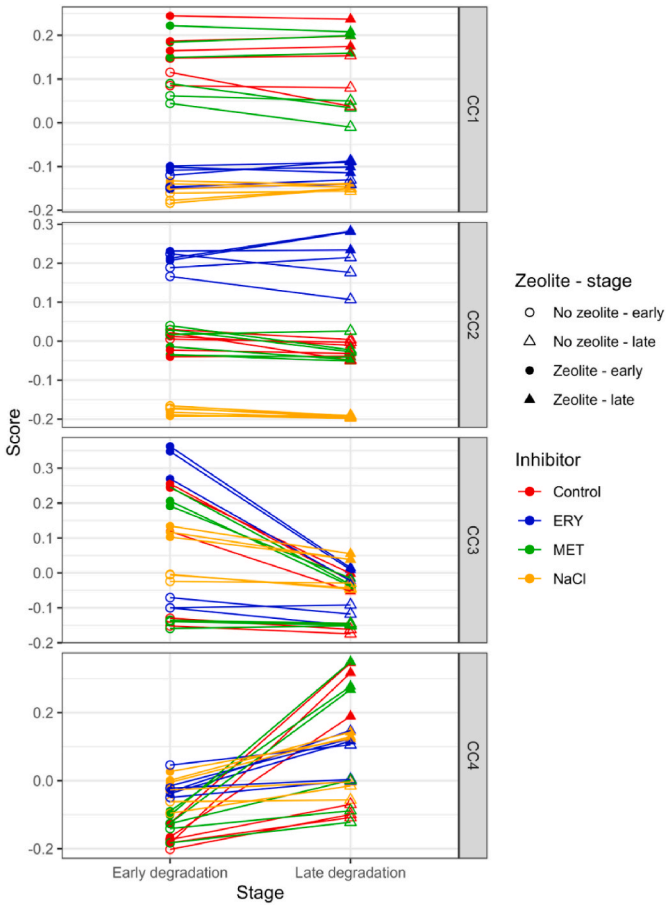


**Fig. 3.** Sample scores on the first 4 components from CCA applied to the microbial data (48 samples in total, 24 digesters multiplied by 2 degradation stages). The color scale indicates the types of inhibitors. Circle and triangle respectively represent early and late degradation stages, with solid ones indicating the addition of zeolite. (For interpretation of the references to color in this figure legend, the reader is referred to the Web version of this article.)

On CC1, the red circles symbolized OTUs characteristic of uninhibited conditions. These populations primarily belonged to a multi-affiliation genus within *Clostridiaceae* family and *Epulopiscium* genus from *Lachnospiraceae* family. The disparities in microbial populations between the inhibited conditions were manifested on CC2. In ERY condition, genera *Clostridium sensu stricto* 1, 2, 5, 13 from *Clostridiaceae* and genus *Herbinix* from *Lachnospiraceae* family showed greater significance, while in the presence of NaCl, *Syner-01* genus from *Synergistaceae* family was the most significant population.

CC3 and CC4 provided valuable insights into zeolite-associated microorganisms. In the early stage, various types of hydrolytic and fermentative bacteria, such as *Cellulosilyticum* from *Lachnospiraceae* family, *Sedimentibacter* from *Sedimentibacteraceae* family, *Clostridium sensu stricto* 17 from *Clostridiaceae* family, and an unidentified genus from *Paludibacteraceae* family, exhibited loadings exceeding 0.8 on CC3. As for the late stage of methane production, CC4 clearly featured certain archaeal populations, including *Methanobacterium* from *Methanobacteriaceae* family, *Methanoculleus* from *Methanomicrobiaceae* family, and *Methanosarcina* from *Methanosarcinaceae* family. Among bacterial populations, *Mesotoga* from *Kosmotogaceae* family exhibited the highest loading, followed by *Syntrophomonas* from *Syntrophomonadaceae* family,

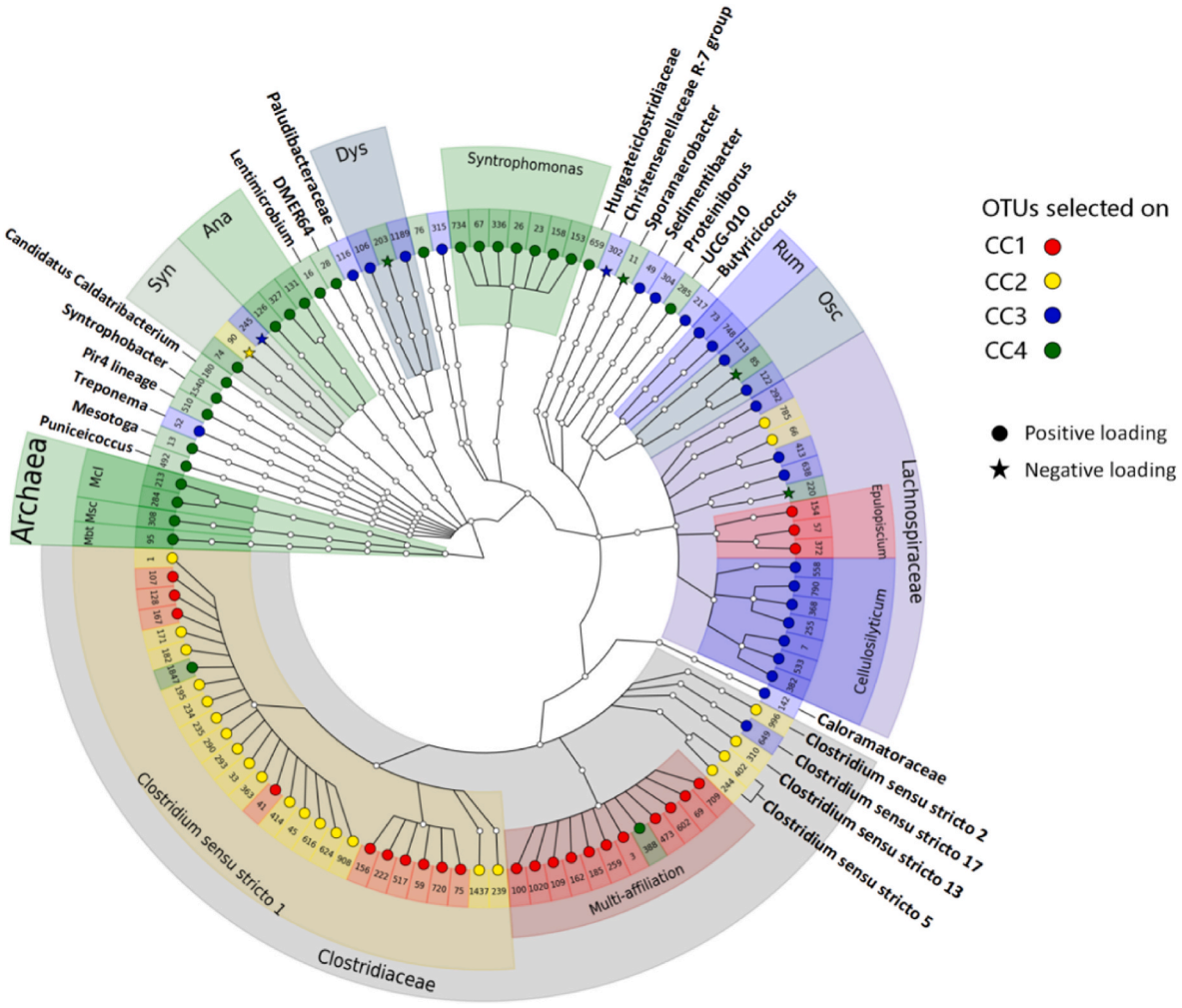


**Fig. 4.** Phylogenetic tree illustrating selected OTUs from CCA. Outer circles and stars depict individual OTUs with their OTU numbers and are colored according to the component on which they are selected. Circles and stars represent positive and negative loadings, respectively. The tree is annotated at different phylogenetic levels. The background color of the sector with annotation is based on the color of all OTUs within that sector. Detailed phylogenetic affiliation, loading value, and the associated CC for each OTU can be found in Table S3. Abbreviations: Mbt, *Methanobacterium*; Msc, *Methanosarcina*; Mcl, *Methanoculleus*; Syn, *Synergistaceae*; Ana, *Anaerolineaceae*; Dys, *Dysgonomonadaceae*; Rum, *Ruminococcaceae*; Osc, *Oscillospiraceae*. (For interpretation of the references to color in this figure legend, the reader is referred to the Web version of this article.)

*Syntrophobacter* from *Syntrophobacteraceae* family, and *Thermovirga* from *Synergistaceae* family, most of which are known as VFAs degraders, with loadings exceeding 0.7. The significant loadings of all these populations suggested their robust association with zeolite, even if also influenced by the inhibitors. Considering the accelerated VFAs consumption and methane production rates in all zeolite conditions, it evidenced that while the impact on each microbial population might vary due to the inhibitors, zeolite overall had a promoting effect on a range of microorganisms.

It is worth mentioning that members of *Sedimentibacteraceae* family could engage in direct interspecies electron transfer (DIET) with electrophilic methanogens such as *Methanosarcina* (Feng et al., 2022). The genera *Syntrophomonas* and *Syntrophobacter* and members from *Kosmotogaceae* and *Synergistaceae* families are associated with propionate oxidation in syntrophy with hydrogenotrophic methanogens including *Methanoculleus* and *Methanobacterium* (Rhee et al., 2021; Westerholm et al., 2022). These microbial populations were highlighted on CC3 and CC4. Therefore, it is plausible that one of the mechanisms through which zeolite took effect is by promoting functional interactions between specific bacteria and methanogens such as DIET and syntrophic propionate oxidation. Furthermore, the acetate produced from propionate degradation also facilitated acetoclastic methanogenesis, which is demonstrated to be the dominant pathway through our isotopic analysis of the biogas when zeolite was added (Chen et al., 2020).

## 4. Conclusion

This study confirmed the generic positive effect of zeolite on AD. Regular monitoring of degradation performance exhibited inhibition of NaCl and ERY on biogas production rate and VFAs degradation. However, zeolite significantly mitigated these inhibitory effects and enhanced degradation performance. Moreover, zeolite also improved AD performance under uninhibited conditions. Microbial community structure analysis displayed typical microorganisms inhibited by NaCl and ERY and those promoted by zeolite, which led to the observed variations in the degradation performance. CCA further illustrated a generic effect of zeolite on microbial populations in both early and late degradation stages, although the individual response of each population was also impacted by the inhibitors. By selecting characteristic OTUs on the identified components, microbial populations closely associated with zeolite were revealed specific to the two degradation stages. Our study therefore suggested the promising application of zeolite to improve the stability of AD.

## Fundings

This work was conducted as part of the STABILICS project supported by the National Research Agency, France (ANR-19-CE43-0003). The funders had no role in study design, data collection and analysis, decision to publish, or manuscript preparation.

## CRediT authorship contribution statement

**Xiaoqing Wang:** Writing – original draft, Visualization, Methodology, Investigation, Formal analysis, Conceptualization. **Vincent Dürr:** Methodology, Formal analysis, Data curation, Conceptualization. **Angéline Guenne:** Methodology, Formal analysis, Data curation. **Laurent Mazéas:** Writing – review & editing, Validation, Supervision. **Olivier Chapleur:** Writing – review & editing, Validation, Supervision, Project administration, Methodology, Funding acquisition, Conceptualization.

## Declaration of generative AI and AI-assisted technologies in the writing process

During the preparation of this work the authors used ChatGPT in order to improve language and readability. After using this tool, the authors reviewed and edited the content as needed and take full responsibility for the content of the publication.

## Declaration of competing interest

The authors declare that they have no known competing financial interests or personal relationships that could have appeared to influence the work reported in this paper.

## Data availability

The sequencing data for this study have been deposited in the European Nucleotide Archive (ENA) at EMBL-EBI under accession number PRJEB65129 (https://www.ebi.ac.uk/ena/browser/view/PRJEB65129).

## Acknowledgment

We are grateful to Véronique Jamilloux, Nadine Derlet, Chrystelle Bureau, and Elodie Gittard for their technical support of this study. Xiaoqing Wang thanks the China Scholarship Council (CSC) for her Ph. D. fellowship.

## Appendix A. Supplementary data

Supplementary data to this article can be found online at https://doi.org/10.1016/j.jenvman.2024.120676.

## References

Abdallah, M., Greige, S., Beyenal, H., Harb, M., Wazne, M., 2022. Investigating microbial dynamics and potential advantages of anaerobic co-digestion of cheese whey and poultry slaughterhouse wastewaters. SCI REP-UK 12, 10529.

Aydin, S., Cetecioglu, Z., Arikan, O., Ince, B., Ozbayram, E.G., Ince, O., 2015. Inhibitory effects of antibiotic combinations on syntrophic bacteria, homoacetogens and methanogens. Chemosphere 120, 515–520.

Balasundaram, G., Vidyarthi, P.K., Gahlot, P., Arora, P., Kumar, V., Kumar, M., Kazmi, A. A., Tyagi, V.K., 2022. Energy feasibility and life cycle assessment of sludge pretreatment methods for advanced anaerobic digestion. BIORESOURCE TECHNOL 357, 127345.

Bouhlel, J., Bouveresse, D.J., Abouelkaram, S., Baéza, E., Jondreville, C., Travel, A., Ratel, J., Engel, E., Rutledge, D.N., 2018. Comparison of common components analysis with principal components analysis and independent components analysis: application to SPME-GC-MS volatolomic signatures. Talanta 178, 854–863.

Buenaño-Vargas, C., Gagliano, M.C., Paulo, L.M., Bartle, A., Graham, A., van Veelen, H.P. J., O'Flaherty, V., 2024. Acclimation of microbial communities to low and moderate salinities in anaerobic digestion. Sci. Total Environ. 906, 167470.

Cardona, L., Levrard, C., Guenne, A., Chapleur, O., Mazéas, L., 2019. Co-digestion of wastewater sludge: choosing the optimal blend. Waste Manage. (Tucson, Ariz.) 87, 772–781.

Cardona, L., Mazéas, L., Chapleur, O., 2021. Zeolite favours propionate syntrophic degradation during anaerobic digestion of food waste under low ammonia stress. Chemosphere 262, 127932.

Casals, E., Barrena, R., Gonzalez, E., Font, X., Sánchez, A., Puntes, V., 2021. Historical perspective of the addition of magnetic nanoparticles into anaerobic digesters (2014-2021). Frontiers in Chemical Engineering, 745610.

Chapleur, O., Mazeas, L., Godon, J., Bouchez, T., 2016. Asymmetrical response of anaerobic digestion microbiota to temperature changes. APPL MICROBIOL BIOT 100, 1445–1457.

Chen, J.L., Ortiz, R., Steele, T.W.J., Stuckey, D.C., 2014. Toxicants inhibiting anaerobic digestion: a review. Biotechnol. Adv. 32, 1523–1534.

Chen, Y., Zeng, Y., Wang, H., Zheng, D., Kamagata, Y., Narihiro, T., Nobu, M.K., Tang, Y., 2020. Different interspecies electron transfer patterns during mesophilic and thermophilic syntrophic propionate degradation in chemostats. Microb. Ecol. 80, 120–132.

Conrad, R., 2005. Quantification of methanogenic pathways using stable carbon isotopic signatures: a review and a proposal. Org. Geochem. 36, 739–752.

Ćwieląg-Piasecka, I., Debicka, M., Medyńska-Juraszek, A., 2021. Effectiveness of carbaryl, carbofuran and metolachlor retention in soils under the influence of different colloid. MINERALS-BASEL 11, 924.

Duan, N., Zhang, D., Khoshnevisan, B., Kougias, P.G., Treu, L., Liu, Z., Lin, C., Liu, H., Zhang, Y., Angelidaki, I., 2020. Human waste anaerobic digestion as a promising low-carbon strategy: operating performance, microbial dynamics and environmental footprint. J. Clean. Prod. 256, 120414.

Escudié, F., Auer, L., Bernard, M., Mariadassou, M., Cauquil, L., Vidal, K., Maman, S., Hernandez-Raquet, G., Combes, S., Pascal, G., 2018. FROGS: find, rapidly, OTUs with galaxy solution. Bioinformatics 34, 1287–1294.

Feng, D., Xia, A., Huang, Y., Zhu, X., Zhu, X., Liao, Q., 2022. Effects of carbon cloth on anaerobic digestion of high concentration organic wastewater under various mixing conditions. J. Hazard Mater. 423, 127100.

Gaballah, M.S., Guo, J., Hassanein, A., Sobhi, M., Zheng, Y., Philbert, M., Li, B., Sun, H., Dong, R., 2023. Removal performance and inhibitory effects of combined tetracycline, oxytetracycline, sulfadiazine, and norfloxacin on anaerobic digestion process treating swine manure. Sci. Total Environ. 857, 159536.

Goldstein, E.J.C., 2000. Review of the in vitro activity of gemifloxacin against Gram-positive and Gram-negative anaerobic pathogens. J ANTIMICROB CHEMOTH 45, 55.

Jannat, M.A.H., Lee, J., Shin, S.G., Hwang, S., 2021. Long-term enrichment of anaerobic propionate-oxidizing consortia: syntrophic culture development and growth optimization. J. Hazard Mater. 401, 123230.

Lee, E., Oliveira, D.S.B.L., Oliveira, L.S.B.L., Jimenez, E., Kim, Y., Wang, M., Ergas, S.J., Zhang, Q., 2020. Comparative environmental and economic life cycle assessment of high solids anaerobic co-digestion for biosolids and organic waste management. Water Res. 171, 115443.

Li, J., Xu, X., Chen, C., Xu, L., Du, Z., Gu, L., Xiang, P., Shi, D., Huangfu, X., Liu, F., 2023. Conductive materials enhance microbial salt-tolerance in anaerobic digestion of food waste: microbial response and metagenomics analysis. Environ. Res. 115779.

Li, L., Peng, X., Wang, X., Wu, D., 2018. Anaerobic digestion of food waste: a review focusing on process stability. BIORESOURCE TECHNOL 248, 20–28.

Li, Q., Liu, Y., Yang, X., Zhang, J., Lu, B., Chen, R., 2020. Kinetic and thermodynamic effects of temperature on methanogenic degradation of acetate, propionate, butyrate and valerate. Chem. Eng. J. 396, 125366.

Liu, Y., Li, X., Tan, Z., Yang, C., 2021. Inhibition of tetracycline on anaerobic digestion of swine wastewater. BIORESOURCE TECHNOL 334, 125253.

Lv, Z., Wu, X., Zhou, B., Wang, Y., Sun, Y., Wang, Y., Chen, Z., Zhang, J., 2019. Effect of one step temperature increment from mesophilic to thermophilic anaerobic digestion on the linked pattern between bacterial and methanogenic communities. BIORESOURCE TECHNOL 292, 121968.

Madigou, C., Lê Cao, K., Bureau, C., Mazéas, L., Déjean, S., Chapleur, O., 2019. Ecological consequences of abrupt temperature changes in anaerobic digesters. Chem. Eng. J. 361, 266–277.

Montalvo, S., Guerrero, L., Borja, R., Sánchez, E., Milán, Z., Cortés, I., Angeles De La La Rubia, M., 2012. Application of natural zeolites in anaerobic digestion processes: a review. Appl. Clay Sci. 58, 125–133.

Munoz, A., Koskinen, W.C., Cox, L., Sadowsky, M.J., 2011. Biodegradation and mineralization of metolachlor and alachlor by Candida xestobii. J. Agric. Food Chem. 59, 619–627.

Nakhli, S.A.A., Delkash, M., Bakhshayesh, B.E., Kazemian, H., 2017. Application of zeolites for sustainable agriculture: a review on water and nutrient retention. Water, Air, Soil Pollut. 228, 1–34.

Nordell, E., Hansson, A.B., Karlsson, M., 2013. Zeolites relieves inhibitory stress from high concentrations of long chain fatty acids. Waste Manage. (Tucson, Ariz.) 33, 2659–2663.

Ogbolu, D.O., Alli, O.A.T., Oluremi, A.S., Onifade, C.O., 2018. Erythromycin resistance determinants in clinical gram positive cocci isolated from Nigerian patients. J. Clin. Diagn. Res. 5–10.

Oliver, J.P., Gooch, C.A., Lansing, S., Schueler, J., Hurst, J.J., Sassoubre, L., Crossette, E. M., Aga, D.S., 2020. Invited review: fate of antibiotic residues, antibiotic-resistant bacteria, and antibiotic resistance genes in US dairy manure management systems. J. Dairy Sci. 103, 1051–1071.

Onodera, T., Syutsubo, K., Hatamoto, M., Nakahara, N., Yamaguchi, T., 2017. Evaluation of cation inhibition and adaptation based on microbial activity and community structure in anaerobic wastewater treatment under elevated saline concentration. Chem. Eng. J. 325, 442–448.

Owusu-Agyeman, I., Plaza, E., Cetecioglu, Z., 2022. Long-term alkaline volatile fatty acids production from waste streams: impact of pH and dominance of Dysgonomonadaceae. BIORESOURCE TECHNOL 346, 126621.
Ozbayram, E.G., Arikan, O., Ince, B., Cetecioglu, Z., Aydin, S., Ince, O., 2015. Acute effects of various antibiotic combinations on acetoclastic methanogenic activity. ENVIRON SCI POLLUT R 22, 6230–6235.
Perez-Perez, T., Pereda-Reyes, I., Correia, G.T., Pozzi, E., Kwong, W.H., Oliva-Merencio, D., Zaiat, M., Montalvo, S., Huilinir, C., 2021. Performance of EGSB reactor using natural zeolite as support for treatment of synthetic swine wastewater. J. Environ. Chem. Eng. 9, 104922.
Poirier, S., Déjean, S., Chapleur, O., 2018. Support media can steer methanogenesis in the presence of phenol through biotic and abiotic effects. Water Res. 140, 24–33.
Puig-Castellví, F., Cardona, L., Bureau, C., Bouveresse, D.J., Cordella, C.B., Mazéas, L., Rutledge, D.N., Chapleur, O., 2020. Effect of ammonia exposure and acclimation on the performance and the microbiome of anaerobic digestion. Bioresour. Technol. Rep. 11, 100488.
Rhee, C., Park, S., Kim, D.W., Yu, S.I., Shin, J., Hwang, S., Shin, S.G., 2021. Tracking microbial community shifts during recovery process in overloaded anaerobic digesters under biological and non-biological supplementation strategies. BIORESOURCE TECHNOL 340, 125614.
Sadecka, Z., Myszograj, S., Sieciechowicz, A., Płuciennik-Koropczuk, E., Włodarczyk-Makuła, M., 2016. Impact of selected insecticides on the anaerobic stabilization of municipal sewage sludge. DESALIN WATER TREAT 57, 1213–1222.
Schnürer, A., Jarvis, Å., 2018. Microbiology of the Biogas Process. Swedish university of agricultural sciences.
Tang, C., Zhang, B., Yao, X., Sangeetha, T., Zhou, A., Liu, W., Ren, Y., Li, Z., Wang, A., He, Z., 2023. Natural zeolite enhances anaerobic digestion of waste activated sludge: insights into the performance and the role of biofilm. J ENVIRON MANAGE 345, 118704.
Ware, A., Power, N., 2017. Modelling methane production kinetics of complex poultry slaughterhouse wastes using sigmoidal growth functions. RENEW ENERG 104, 50–59.
Westerholm, M., Calusinska, M., Dolfing, J., 2022. Syntrophic propionate-oxidizing bacteria in methanogenic systems. FEMS Microbiol. Rev. 46, fuab57.
Xiao, H., Zhang, D., Tang, Z., Li, K., Guo, H., Niu, X., Yi, L., 2022. Comparative environmental and economic life cycle assessment of dry and wet anaerobic digestion for treating food waste and biogas digestate. J. Clean. Prod. 338, 130674.
Yang, G., Xu, H., Luo, Y., Hei, S., Song, G., Huang, X., 2023. Novel electro-assisted micro-aerobic cathode biological technology induces oxidative demethylation of N, N-dimethylformamide for efficient ammonification of refractory membrane-making wastewater. J. Hazard Mater. 442, 130001.
Yin, Q., Gu, M., Wu, G., 2020. Inhibition mitigation of methanogenesis processes by conductive materials: a critical review. BIORESOURCE TECHNOL 317, 123977.
Zhang, Z., Li, C., Wang, G., Yang, X., Zhang, Y., Wang, R., Angelidaki, I., Miao, H., 2023. Mechanistic insights into $Fe_3O_4$-modified biochar relieving inhibition from erythromycin on anaerobic digestion. J ENVIRON MANAGE 344, 118459.
Zheng, Y., Quan, X., Zhuo, M., Zhang, X., Quan, Y., 2021. In-situ formation and self-immobilization of biogenic Fe oxides in anaerobic granular sludge for enhanced performance of acidogenesis and methanogenesis. Sci. Total Environ. 787, 147400.